Chinese Journal of Chemical Engineering 94 (2026) 156–171

Contents lists available at ScienceDirect

Chinese Journal of Chemical Engineering

journal homepage: www.elsevier.com/locate/CJChE

Full Length Article

An interpretable ensemble learning framework based on Bayesian optimization for the optimal design of ammonia decomposition catalysts

Zhao Wang, Jingsong Guan, Jun Hu, Qiwen Guo, Dawei Zhang, Qingchun Yang *

School of Chemistry and Chemical Engineering, Hefei University of Technology, Hefei 230009, China

ARTICLE INFO

Article history:
Received 9 September 2025
Received in revised form
7 January 2026
Accepted 8 January 2026
Available online 19 February 2026

Keywords:
Ammonia decomposition
Ensemble learning
Optimization
Catalyst
Hydrogen production

ABSTRACT

Green ammonia offers a viable hydrogen carrier due to its high energy density, established infrastructure, and cost-effectiveness. However, the decomposition process for hydrogen production relies on highly efficient catalysts. This study aims to overcome experimental limitations in catalyst design by developing a Bayesian optimization-based interpretable ensemble learning framework for multi-objective optimization of ammonia decomposition catalysts. A dataset covering the intrinsic properties of catalysts, preparation parameters, and reaction conditions for ammonia decomposition is constructed to develop six various ensemble learning models. The hyperparameters of these models are automatically and optimally configured using the Bayesian optimization-based Optuna method. The results demonstrate the effectiveness of this hyperparameter automatic optimization strategy, as the average R^2 across the six models improved by 0.086 compared to the pre-optimization values. In particular, the CatBoost model emerges as the optimal model with test $R^2 > 0.9188$. The Shapley additive explanations reveal the regulatory mechanism of performance by reaction conditions (with a contribution of 48.14%, where temperature and space velocity are dominant) and intrinsic characteristics of the catalyst (33.79%). The partial dependence plots analyses are further conducted to expound the effect of these key parameters on the catalytic performance. The optimal model is integrated with the reference vector guided evolutionary algorithm to minimize the total metal content while maximizing the space-time yield of hydrogen in ammonia decomposition catalysts. Three newly optimized catalysts demonstrate superior performance, offering an improved efficiency-cost balance compared to existing catalysts. External validation with unseen data further confirms the model's robustness, with prediction errors <5.06%.

© 2026 The Chemical Industry and Engineering Society of China, and Chemical Industry Press Co., Ltd. All rights are reserved, including those for text and data mining, AI training, and similar technologies.

1. Introduction

The global climate change and the increasing demand for energy have significantly accelerated the need for renewable energy sources. As an environmentally friendly and sustainable resource, green hydrogen has garnered widespread attention worldwide. However, due to its low volumetric energy density and high risks, the development of an efficient and convenient transportation carrier remains crucial, posing a major bottleneck to its large-scale industrial application [1]. In this context, on-site ammonia decomposition has emerged as a promising solution to address the challenges of hydrogen storage and transportation, holding significant implications for energy transition and environmental sustainability [2].

Ammonia (NH_3), with a hydrogen content of up to 17.6%, serves as a highly efficient hydrogen carrier. It offers several advantages, including high energy density, ease of storage and transportation, existing infrastructure, and carbon-neutral potential [3]. Furthermore, the cost of ammonia from source-to-tank (at 4.50 USD per gallon of gasoline equivalent) is the lowest among comparable fuels, being approximately 18% lower than that of methanol and about 31% lower than that of hydrogen [4]. As the development of renewable energy continues to gain momentum, the feasibility of

This article is part of a special issue entitled: Sino-Thai Frontiers of Green Chemical Engineering published in Chinese Journal of Chemical Engineering.

* Corresponding author.
E-mail address: ceqcyang@hfut.edu.cn (Q. Yang).

https://doi.org/10.1016/j.cjche.2026.01.006
1004-9541/© 2026 The Chemical Industry and Engineering Society of China, and Chemical Industry Press Co., Ltd. All rights are reserved, including those for text and data mining, AI training, and similar technologies.

this solution becomes increasingly evident [5]. In particular, the concept of "green ammonia" has attracted considerable attention, further highlighting the potential of ammonia-based hydrogen transportation to a sustainable energy future [6].

However, despite the growing interest, there remains a significant gap between the depth of existing research and the practical application of on-site hydrogen production through ammonia decomposition [7]. Firstly, the current ammonia decomposition reaction requires to be carried out at a temperature exceeding 700 °C to achieve complete conversion. This is because the activation energy for the cleavage of the N—H bond and the desorption of nitrogen is relatively high. Although the decomposition of ammonia into hydrogen is thermodynamically favorable above 400 °C, the reaction kinetics remain sluggish [8]. Such high temperatures will reduce the energy efficiency of on-site hydrogen production and make it more dangerous. Secondly, since the decomposition reaction is endothermic, a large amount of energy input is also required to maintain the reaction conditions [9]. Therefore, given that the storage technology for liquid or solid ammonia is already mature, the key strategy for large-scale utilization of ammonia as a hydrogen carrier lies in designing and constructing efficient ammonia decomposition catalysts to lower the reaction temperature, enhance hydrogen production efficiency, and reduce energy costs.

To this issue, some researchers have proposed planning and optimization designs for ammonia decomposition from the perspectives of size effect, alkalinity adjustment, interaction between metals and carriers, and alloy effect, based on experimental methods and tools [6,10,11]. These experimental approaches have provided valuable insights into the underlying mechanisms and have proven effective in identifying key factors influencing ammonia decomposition efficiency. However, despite their success, these methods exhibit notable limitations, particularly in terms of scalability, high cost, and the inability to fully capture the complex, nonlinear interactions between multiple variables involved in the ammonia decomposition process [12]. Furthermore, the experimental approaches often require extensive time and resources to optimize various parameters, making them less suitable for rapid and large-scale applications [13]. In addition, the performance evaluation of catalysts involves multiple aspects. Relying solely on experimental methods makes it difficult to optimize them simultaneously, often leading to getting stuck in local optima [14].

To overcome these challenges, there is a growing need for more advanced approaches, such as machine learning (ML) techniques, which have shown great potential in optimizing complex processes [15,16]. By leveraging ML models, researchers can analyze large datasets, identify hidden patterns, and predict optimal operating conditions more efficiently [17]. Machine learning has the ability to handle the vast number of variables and their interactions, enabling the development of more accurate, real-time optimization strategies that can accelerate the process of ammonia decomposition [18]. This shift towards data-driven methods represents a crucial step toward improving the scalability and efficiency of ammonia-based hydrogen carriers in the context of green energy solutions. For example, Zahrt *et al.* [17] successfully achieved highly accurate predictions of enantioselectivities using machine learning, and believed that the ability to predict selective catalysts could revolutionize how chemists choose and fine-tune chiral catalysts, shifting the approach from one driven by empirical methods to one guided by mathematical models. Guo *et al.* [19] developed multiple machine learning prediction systems for catalyst performance forecasting. Through a three-stage modeling comparison, the Gradient Boosting Regression model, a type of ensemble learning model, was found to perform the best on the test set. Similarly, when analyzing and comparing the performance of kernel learning algorithms, neural network algorithms, and ensemble learning algorithms for predicting the performance of biomass pyrolysis catalysts, Chen *et al.* [20] found that the ensemble learning model exhibited the highest prediction accuracy. Similar trends were also observed for the processes of supercritical water gasification and photocatalytic pollutant degradation, where ensemble models demonstrated the best predictive performance [21,22].

These studies highlight the applicability and superiority of ensemble learning in catalyst prediction. However, they have not fully explored the nuances of the various ensemble learning algorithms and their comparative performance across different catalytic systems. Furthermore, the selection of the best model is usually based on relatively small specific datasets or certain catalytic systems, which may not generalize well to other complex catalytic processes, such as ammonia decomposition. Moreover, the predictive performance of various ensemble learning models is heavily influenced by their hyperparameter configurations. However, conventional hyperparameter optimization techniques, such as grid search and random search, tend to be time-intensive and computationally costly, particularly when applied to complex catalytic systems involving a large number of variables [23]. Additionally, these methods do not always guarantee the identification of the optimal set of parameters, as they may fail to efficiently explore the vast search space [24]. Given the computational cost and potential inefficiency of these traditional approaches, there is a growing need for automated hyperparameter tuning strategies. Bayesian optimization, for example, offers a more efficient approach by using probabilistic models to guide the search process and adaptively focus on the most promising regions of the hyperparameter space [25]. This method not only reduces the computational burden but also improves the likelihood of finding the optimal model parameters [26]. In addition, one of the significant challenges with ensemble learning models is the lack of interpretability [27]. While these models often provide high predictive accuracy, they do so in a "black-box" manner, which makes it difficult to understand the underlying reasons behind their predictions [24]. This lack of transparency is particularly problematic when it comes to scientific applications like catalyst optimization, where understanding the rationale behind model predictions is crucial for making informed decisions about experimental design and optimization [14]. Therefore, it is crucial to incorporate interpretability and automated hyperparameter optimization into ensemble learning algorithms for offering a more reliable and transparent methodology for catalyst optimization, especially in complex catalytic processes such as ammonia decomposition.

To address these issues, this study aims to propose a Bayesian optimization-based interpretable ensemble learning framework for the multi-objective optimization design of ammonia decomposition catalysts. The main contributions of this study are: (a) Develop an interpretable ensemble learning framework that incorporates Bayesian optimization techniques to efficiently search the hyperparameter space and optimize model performance. (b) Evaluate the prediction accuracy, generalization capability, and interpretability of various ensemble learning algorithms to identify the most effective model for the ammonia decomposition process; (c) Apply interpretability approaches to elucidate the model's decision-making process, quantify the contributions and interaction mechanisms of input features, and thereby enhance the understanding of key features that drive catalyst performance; and (d) Integrate the preferred ensemble learning model with a multiobjective optimization algorithm to optimize and predict ammonia decomposition catalyst by balancing their

hydrogen production capacity against cost considerations. By combining the power of Bayesian optimization with interpretable ensemble models, this research will not only improve predictive accuracy but also ensure that the insights gained from the model are actionable and scientifically valuable for real-world applications.

2. Materials and Methods

An interpretable ensemble learning framework based on Bayesian optimization is proposed for the multi-objective optimization design of ammonia decomposition catalysts, as illustrated in Fig. 1. First, a dataset of ammonia decomposition catalysts is constructed for the modeling and optimization of catalyst performance. This dataset consists of catalyst intrinsic parameters, preparation conditions, reaction conditions, and targets of the ammonia decomposition catalysts. Second, feature correlation analysis methods, such as Pearson correlation and Spearman rank correlation, are employed to identify the most influential features for model performance and remove redundant features. Third, various ensemble learning models for ammonia decomposition catalysts are developed and optimized through an automated hyperparameter tuning method based on Bayesian optimization. Fourth, the optimal model, determined through multi-dimensional comparisons, is explained both globally and locally using Shapley additive explanations (SHAP) and partial dependence analysis. Finally, the optimal model is integrated with the optimization algorithm to predict and optimize ammonia decomposition catalysts, aiming to achieve the highest space-time yield of hydrogen with minimal cost.

2.1. Construction of the ammonia decomposition dataset

This study analyzes the catalytic conversion of ammonia through a systematic research methodology. Literature retrieval is rigorously conducted based on the Web of Science database using combined keywords (*e.g.*, “ammonia decomposition”, “catalytic conversion”, “hydrogen production”), followed by a three-tiered manual screening protocol: (i) initial screening based on titles and abstracts; (ii) secondary screening for full-text relevance; (iii) final screening for data integrity. A total of 69 core publications that met the data extraction criteria are ultimately selected as the foundation for this research. In this regard, a standardized dataset containing 1479 records was constructed in this study. All data are systematically structured using standardized extraction templates and verified through cross-referencing.

Based on the ammonia decomposition dataset established through the literature screening process, the catalyst descriptors are systematically classified catalyst parameters into three distinct categories based on their functional attributes and disciplinary relevance: intrinsic catalyst properties, catalyst preparation parameters, and reaction conditions, as shown in Table 1.

Specifically, intrinsic catalyst properties include chemical composition (active component, support, and metal loading), physical structure (specific surface area, crystallite size, pore volume, pore diameter, and crystallinity), and elemental attributes (atomic radius, electron affinity, and atomic weight). These features systematically characterize the static attributes of catalysts from the atomic scale to the mesoscopic scale. It should be noted that in this article, the main active metal is designated as

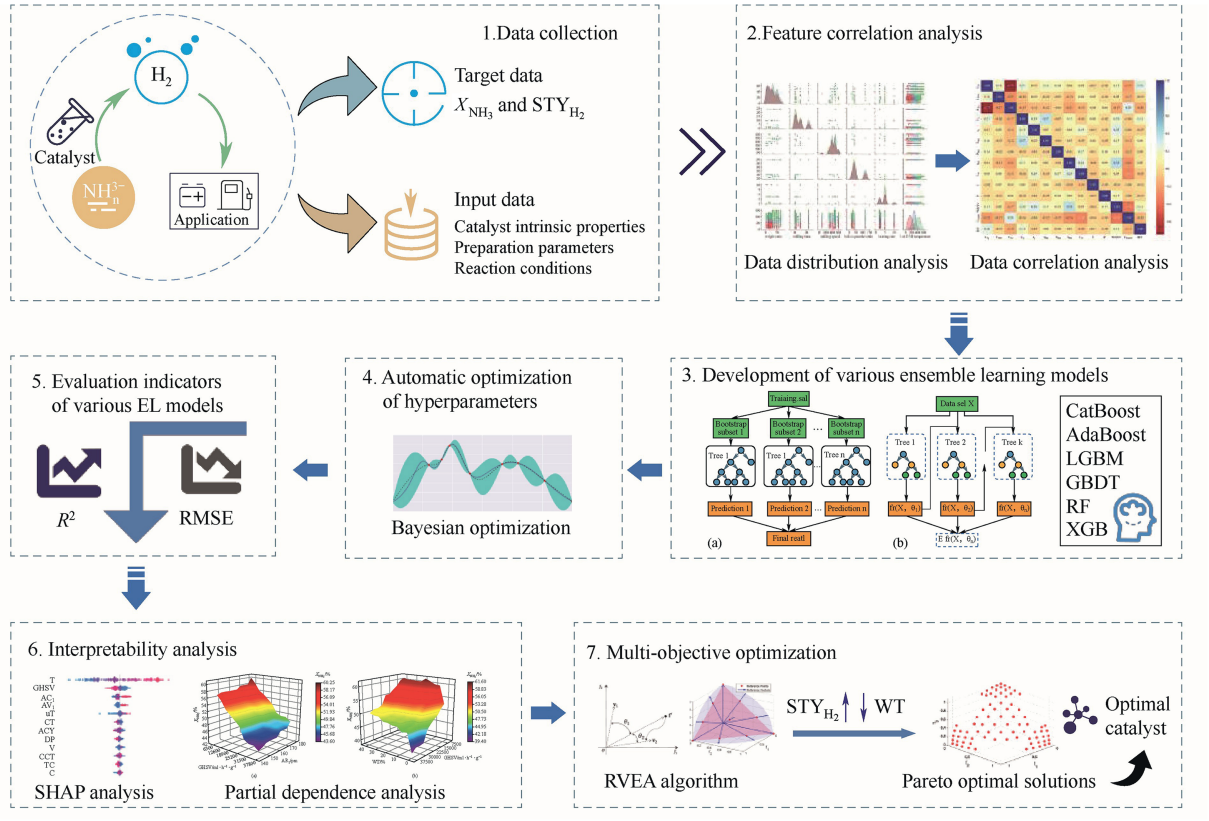


Fig. 1. Schematic diagram of the proposed interpretable ensemble learning framework based on Bayesian optimization for the multi-objective optimization design of NH_3 decomposition catalysts.

Table 1
Input and output feature of the ammonia decomposition dataset.

	Feature name	Unit	Feature name	Unit
Input	Active component (AC)	–	Reduction time (TR)	h
	Atomic radius (AR)	pm	Total metal loading (WT)	%
	Electron affinity (EA)	$kJ \cdot mol^{-1}$	Average crystallite size (ACS)	nm
	Atomic weight (AW)	–	Catalyst crystallinity index (CCI)	–
	Carrier (C)	–	Specific surface area (BET)	$m^2 \cdot g^{-1}$
	Preparation method (PM)	–	Catalyst pore volume (V)	$cm^3 \cdot g^{-1}$
	Calcination temperature (CT)	°C	Average pore diameter (DP)	nm
	Calcination time (TC)	h	Reaction temperature (T)	°C
	Reduction temperature (RT)	°C	Gas hourly space velocity (GHSV)	$ml \cdot h^{-1} \cdot (g\ cat)^{-1}$
Output	Ammonia conversion (X_{NH_3})	%	Space-time yield of hydrogen (STY_{H_2})	$mmol \cdot (g\ cat)^{-1} \cdot min^{-1}$

AC_1, while the secondary active metal or additive component is uniformly designated as AC_2. This can efficiently and effectively manage the high heterogeneity of reported data in the literature and alleviate the potential problem of data sparsity. This method is widely applied in situations where the role or content of bimetallic catalysts is difficult to determine. For instance, in some literature, the second metal is regarded as the active component; while in others, multiple additives are included, but the standardized information such as their exact loading amounts, doping methods, or specific chemical forms is often reported inconsistently. By uniformly categorizing these diverse secondary components into the AC_2 feature, it can provide a more robust, dense, and moderately dimensional feature representation for model training, thereby avoiding the problem of overly high feature dimension and data sparsity caused by treating each specific additive as an independent parameter. Catalyst preparation parameters include the preparation method and the synthesis conditions for calcination (temperature/time) and reduction (temperature/time). These parameters enable targeted regulation of the dynamic structural evolution of the catalyst throughout the synthesis process by modulating thermodynamic phase transformations during its preparation. Reaction conditions comprise the reaction temperature and the gas hourly space velocity (GHSV). The reaction temperature influences the intrinsic reaction rate constant through the Arrhenius equation, whereas the GHSV affects the surface coverage of reactants by determining their residence time. These two parameters jointly establish the macroscopic operational limits of the catalytic system. The nomenclature and corresponding abbreviations for all dataset features are detailed in Table 1.

2.2. Feature correlation analysis

Feature correlation analysis is employed to assess the statistical association between two variables. The Pearson's correlation coefficient (r) and Spearman's rank correlation coefficient (ρ) are adopted to quantitatively evaluate the degree of correlation among features within the dataset. The former assesses the strength and direction of the linear relationship between two continuous variables. The latter is a non-parametric statistical method used to assess the correlation between the ranks or orders of two variables. Similar to Pearson's correlation coefficient, Spearman's correlation coefficient also ranges from −1 to 1. However, it is computed based on the ranks of the variable values rather than their original magnitudes. These analyses quantitatively reveal redundancy patterns and identify high-leverage predictors critical for reaction optimization. Resultant correlation matrices directly inform feature selection and preprocessing strategies for subsequent machine learning workflows.

2.3. Development and automatic optimization of EL model

To identify the optimal predictor for the ammonia decomposition process, six ensemble learning models are systematically developed and automatically optimized: Categorical Boosting (CatBoost), Adaptive Boosting (AdaBoost), Light Gradient Boosting Machine (LGBM), Gradient Boosting Decision Trees (GBDT), Random Forest (RF), and eXtreme Gradient Boosting (XGB), respectively.

2.3.1. Development of various ensemble learning models

Accurate prediction of catalytic performance requires accommodating diverse relationships within complex datasets. As no single ensemble learning algorithm universally captures all underlying data patterns, this study strategically selects six representative ensemble learning approaches to span key variants of the gradient boosting framework, adaptive boosting mechanisms, and parallel ensemble paradigms: CatBoost, AdaBoost, LGBM, GBDT, RF, and XGB, respectively.

The primary rationale for selecting these six algorithms lies in their capacity to systematically address complex nonlinear patterns within the structure-performance relationships of ammonia decomposition catalysts. For instance, GBDT provides foundational architecture using additive modeling to iteratively fit residual errors; XGBoost incorporates L2 regularization and second-order Hessian approximation to navigate bias-variance tradeoffs; LGBM revolutionizes tree growth *via* histogram-based feature binning and depth-constrained leaf-wise expansion to accelerate training process [28]; CatBoost specifically addresses categorical features (*e.g.*, active metal types) through ordered target encoding and symmetric tree structures to suppress prediction drift [29]. These four algorithms achieve complementary specializations as variants of gradient boosting. For adaptive boosting, AdaBoost leverages exponential loss weighting to dynamically recalibrate instance importance, constructing error-adaptive classification boundaries through sequential weak learner fusion [30]. Finally, Random Forest applies bootstrap aggregation with random subspace sampling to parallelize decorrelated decision trees, establishing robust baselines for high-dimensional feature selection [31].

2.3.2. Automatic optimization of hyperparameters

Hyperparameters, as predefined regulatory variables, directly influence the learning process and structural development of models during training [32]. Systematic hyperparameter tuning not only enhances predictive accuracy and generalization capability but also improves training efficiency and accelerates convergence [33]. Therefore, the Bayesian optimization-based Optuna optimizer is proposed to achieve a balanced trade-off among prediction accuracy, compliance with complex

constraints, and the reduction of risks associated with manual intervention in this study. This optimizer achieves efficient hyperparameter search by integrating the Tree-structured Parzen Estimator (TPE) sampler and Successive Halving Algorithm (SHA) pruner advantages on the Bayesian optimization based Optuna framework. The detailed information of the key hyperparameter of the ML models is listed in Table S1.

2.3.3. Evaluation indicators of various EL models

A dual evaluation framework combining the coefficient of determination (R^2) and root mean square error (RMSE) is established to comprehensively evaluate ensemble learning (EL) model performance. Specifically, R^2 quantifies the proportion of variance in target variables explained by the model, as formulated in Eq. (1). RMSE measures absolute prediction deviation as the square root of the mean squared residuals, as indicated in Eq. (2). This framework synergizes an interpretable statistical measure (R^2) with a scale-independent error metric (RMSE) to holistically assess the performance accuracy and limitation of various ensemble learning models.

$$\mathrm{RMSE} = \sqrt{\frac{1}{n}\sum_{i=1}^{n}(y_i - \widehat{y}_i)^2} \tag{1}$$

$$R^2 = 1 - \frac{\sum_{i=1}^{n}(\widehat{y}_i - \overline{y})^2}{\sum_{i=1}^{n}(y_i - \overline{y})^2} \tag{2}$$

where y_i and $\hat{y}$ refer to the actual observed value of the i-th sample point and its predicted value by the model.

2.4. Interpretability analysis

The SHapley Additive exPlanations (SHAP) and Partial Dependence Plots (PDPs) analyses are conducted to explore the significance of ammonia decomposition catalyst features and the interaction mechanism at multiple scales. The SHAP method operates on Shapley values derived from cooperative game theory, satisfying axiomatic properties of local accuracy, missingness, and consistency. It constructs an additive feature attribution model to decompose the model's predicted value into a linear combination of the base value and the SHAP values of each feature, thereby providing interpretable prediction decompositions at the individual sample level. Hence, the SHAP quantifies feature contributions and identifies descriptor-property relationships critical for catalyst design. Complementarily, the PDP method evaluates macro-scale reaction effects through conditional expectation. It quantifies the marginal contribution of independent variables to model predictions by calculating the conditional expected value of the target variable under specific feature combinations. This method can effectively identify nonlinear relationships and synergistic/antagonistic effects among features. This synergistic framework establishes a multi-dimension interpretability paradigm, enabling unprecedented decoding of catalytic reaction networks beyond black-box limitations.

2.5. Multi-objective optimization

Space-time yield of hydrogen ($\mathrm{STY_{H_2}}$) is a decisive economic indicator for the design of catalytic reactors since it is directly related to the production capacity and the cost of hydrogen [34]. However, its improvement usually relies on increasing the loading of precious metals, which leads to a super linear increase in material costs, reactor volume, and energy consumption. Moreover, while increasing the metal loading can typically enhance the number of active sites, exceeding a certain threshold may instead result in issues such as sintering and a decrease in dispersion. Therefore, this paper proposes the reference vector guided evolutionary algorithm (RVEA) to optimize the ammonia decomposition catalyst, aiming to find a new type of highly efficient catalyst that minimizes the total metal content while maximizing the space-time yield of hydrogen, as indicated in Eqs. (3)–(5).

$$\text{Maximize}: f_1(x) = \mathrm{STY_{H_2}}(x) \tag{3}$$

$$\text{Minimize}: f_2(x) = \mathrm{WT}(x) \tag{4}$$

$$\mathrm{lb}_i \le x_i \le \mathrm{ub}_i, i = 1, 2, \ldots, 21 \tag{5}$$

where x refers to the input features listed in Table 1.

The RVEA algorithm is an advanced multi-objective optimization framework based on decomposition strategy, with its core lying in balancing the convergence and diversity of solutions through a dynamic reference vector system. This architecture delivers salient advantages, such as Enhanced high-dimensional optimization capability; Theoretically guaranteed diversity maintenance; and Adaptive resource allocation [35]. Compared with the traditional genetic algorithm, RVEA demonstrates significant advantages in handling multi-objective problems. The former mainly relies on the crowding distance mechanism to maintain population diversity. However, when the number of objective dimensions increases, the efficiency of the crowding distance in distinguishing the diversity of solutions significantly decreases, making it difficult for the algorithm to effectively approach and cover the entire Pareto front. The RVEA algorithm guides the search process by introducing uniformly distributed reference vectors and demonstrates stronger robustness and scalability in balancing convergence and diversity through scalarization methods such as Angle Penalized Distance [35]. This strategy based on reference vectors can maintain the uniform distribution of solutions more effectively, and it can offer better performance even when the objective function is not well normalized or the geometric structure of the Pareto front is complex.

To achieve the minimum metal content while maximizing the hydrogen generation rate of the ammonia decomposition catalyst, the optimization process combines the design of catalyst components with the optimization of process parameters. The lower limit (lb) and upper limit (ub) of the 17 input features are taken as the constraint conditions as shown in Eq. (5). Finally, the Technique for Order Preference by Similarity to Ideal Solution (TOPSIS) is employed for analyzing and ranking the results of multi-objective optimization. As a result, the techno-economically optimal catalyst can be identified by evaluating their relative proximity to ideal benchmarks.

3. Results and Discussion

3.1. Visualization and analysis of the established ammonia decomposition dataset

The box plot visually presents the distribution density of each characteristic parameter and the characteristics of outliers. Furthermore, it reveals statistically significant distribution differences among different categories through interquartile range and outlier distribution, providing an important basis for subsequent feature correlation analysis. Therefore, box plots are employed to visualize the distribution of continuous variables in the established

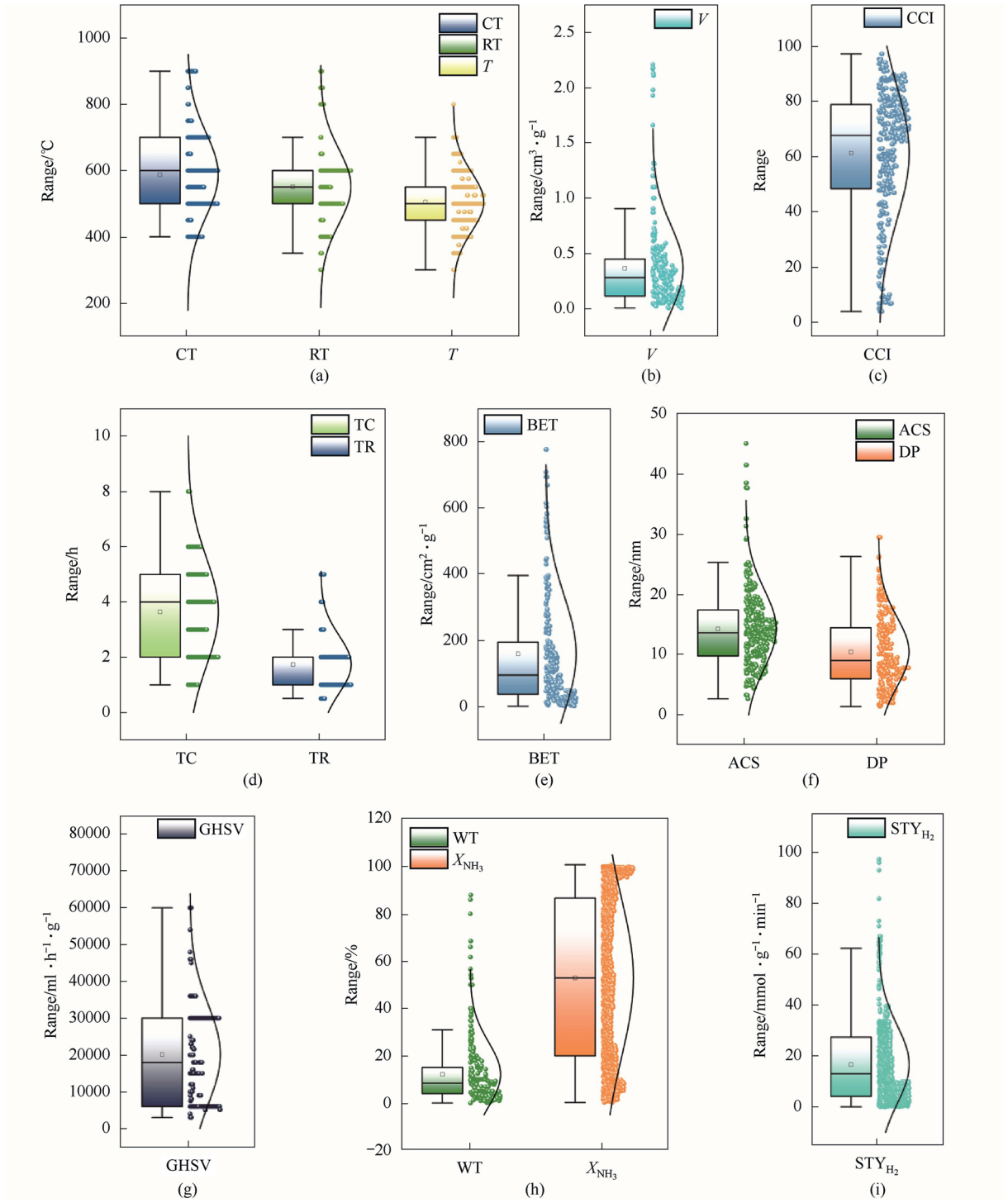


Fig. 2. Box plots of the distribution of various input and output features of the established ammonia decomposition catalysts dataset: (a) CT, RT, and T; (b) V; (c) CCI; (d) TC and TR; (e) BET; (f) ACS and DP; (g) GHSV; (h) WT, and X_{NH_3}; and (i) STY_{H_2}, respectively.

ammonia decomposition dataset, as shown in Fig. 2(a)–(i). To prepare the ammonia decomposition catalysts, the calcination temperatures (CT) are predominantly in the range of 500–700 °C; while the reduction temperatures (RT) are maintained within the range of 400–600 °C; and the temperature (*T*) is mainly distributed in the range of 400–600 °C, as indicated in Fig. 2(a). The pore volume (*V*) is concentrated in the low-value range of 0–1 $cm^3 \cdot g^{-1}$, as depicted in Fig. 2(b). The crystallinity index (CCI) mainly falls within the range of 40-80, as depicted in Fig. 2(c). Corresponding durations for calcination (TC) not exceeding 5 h; while the reduction durations (TR) are strictly controlled at 1 to 2 h, as indicated in Fig. 2(d). The specific surface area (BET) shows a wide distribution from 0 to 200 $m^2 \cdot g^{-1}$, as illustrated in Fig. 2(e). The average crystal grain size (ACS) is stably distributed within 10–20 nm; and the average pore diameter (DP) is mainly distributed within 10–20 nm, as illustrated in Fig. 2(f). The gas hourly space velocity (GHSV) shows a wide

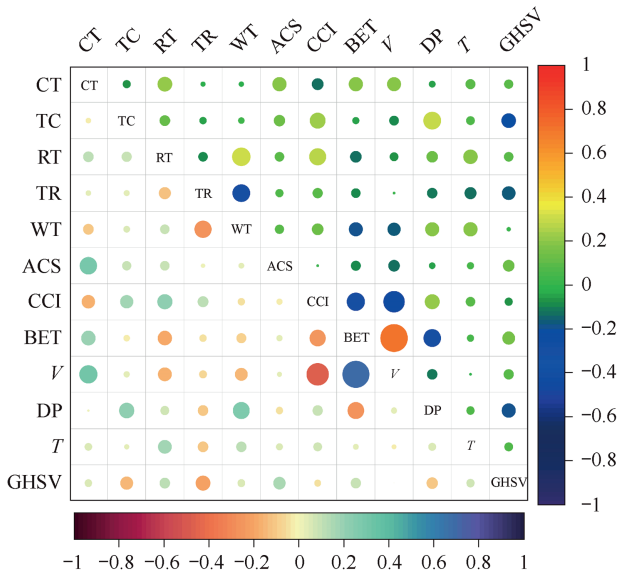


Fig. 3. Heat map of the Pearson correlation and Spearman rank correlation analyses of the numerical features in the ammonia decomposition dataset.

distribution from 5000 to 30000 ml·h^{-1}·(g cat)$^{-1}$, as depicted in Fig. 2(g). The total metal loading (WT) is concentrated in the range of 0% to 20%; and the ammonia conversion ratio (X_{NH_3}) is concentrated in the intervals of 20% to 80%, as presented in Fig. 2(h). Under the influence of these input features, the space-time yield of hydrogen (STY_{H_2}) is concentrated in the interval of 0–20 mmol·(g cat)$^{-1}$·min^{-1}, as presented in Fig. 2(i).

In addition, the constructed dataset covers a variety of metal-based catalysts, as shown in Fig. S1. Ni, Ru, and Co account for significant proportions in the main active components (AC_1), being 39.35%, 25.49%, and 20.22%, respectively. This is in line with their widely studied and applied status in the field of ammonia decomposition catalysis. Moreover, the AC_1 in the dataset also contains other components with emerging research value such as Fe (7.10%), Cu (3.38%), and Zn (1.69%), reflecting the broad diversity in catalyst design. Results also indicates that a large number of ammonia decomposition catalysts do not contain AC_2, while the few that do mainly include Mo, Co, and K. Therefore, these visualization results of the continuous and categorical variables not only reveal the distinct distribution characteristics of each feature but also lay the foundation for building robust and accurate predictive models of ammonia decomposition process.

To further visually demonstrate the interrelationships among the features, the Pearson correlation and Spearman rank correlation methods are applied to analyze the numerical features in the ammonia decomposition dataset, as shown in Fig. 3. The lower left section presents the results of the Pearson correlation analysis, while the upper right section displays the findings of the Spearman rank correlation analysis. Pearson and Spearman correlation coefficients between all feature pairs are below 0.5, except for the statistically significant association between BET surface area and pore volume. This high correlation stems from the intrinsic connection between pore volume and BET surface area in characterizing the pore structure of materials. Pores are the fundamental elements that constitute the internal surface area of materials; an increase in pore volume typically indicates a more developed or complex internal pore network, which significantly enhances the available surface area for adsorption. Therefore, these two parameters jointly and complementarily reflect the characteristics of the porous structure of materials. However, the Pearson and Spearman rank correlation coefficients between BET surface area and pore volume are only 0.69 and 0.71, which indicate only a moderate association and do not imply multicollinearity requiring feature elimination. Therefore, all these input features are used to develop ensemble learning models for the high-precision screening and optimization of ammonia decomposition catalysts.

3.2. Determination of the optimal model for ammonia decomposition catalysts

The optimal model for the ammonia decomposition process is determined by comparing the R^2 and RMSE of these six ensemble-learning models.

3.2.1. Hyperparameter optimization convergence and global optimal identification

The hyperparameter configurations for all six ensemble models are optimized using the Optuna framework, which iteratively explores predefined parametric spaces through sequential trials. Each trial evaluates candidate parameters by minimizing the loss function of RMSE. As shown in Fig. 4(a)–(f), the multi-colored dispersion points represent the global optimal solutions recorded during the parameter optimization process of each model, and the spline interpolation curve at the bottom reveals the distribution pattern of historical loss function values in the iterative space. After 200 iterations, all models achieved asymptotic convergence with stabilized RMSE losses, which indicates that the optimization process has reached a convergent state. Especially, the loss function values of the CatBoost model are the lowest and stabilize around 0.22. Moreover, those of the AdaBoost, LGBM, GBDT, RF, XGB models around 0.35, 0.25, 0.23, 0.38, and 0.25, respectively. Therefore this convergence behavior confirms Optuna's efficacy in locating near-global optima within bounded computational budgets. The optimal hyperparameters of each model are shown in Table S2.

3.2.2. Analysis of the effectiveness of the automatic hyperparameter tuning strategy

By comparing the predictive performance before and after hyperparameter optimization, it can be found that the R^2 values of all models are significantly increased after hyperparameter adjustment, indicating a notable improvement in the goodness of fit of the models, as indicated in Fig. 5(a). In particular, the R^2 of the AdaBoost and GBDT models is increased from 0.5692 to 0.8535 and from 0.8043 to 0.9139, respectively. This significant performance improvement indicates that the AdaBoost model is highly sensitive to the selection of hyperparameters and may have been in a clearly under-optimized state before parameter tuning. Through meticulous fine-tuning, the model's potential predictive power has been fully unleashed. Moreover, comparing the changes in RMSE values of the six models before and after hyperparameter tuning, the results also prove the effectiveness of the hyperparameter automatic optimization strategy adopted in this study since the average RMSE of the six models decreased by 2.0677 compared to before optimization, as indicated in Fig. 5(b). For instance, the RMSE of the AdaBoost and GBDT are reduced from 15.2117 to 9.1112 and from 10.2773 to 7.1931 compared with that of before hyperparameter tuning. More results regarding the performance of the automatic optimization strategy in enhancing the prediction of the conversion rate and space-time yield of hydrogen of the ammonia decomposition process are placed in Fig. S2. Therefore, the proposed Bayesian-based Optuna approach can indeed significantly enhance the prediction accuracy of the ammonia decomposition models.

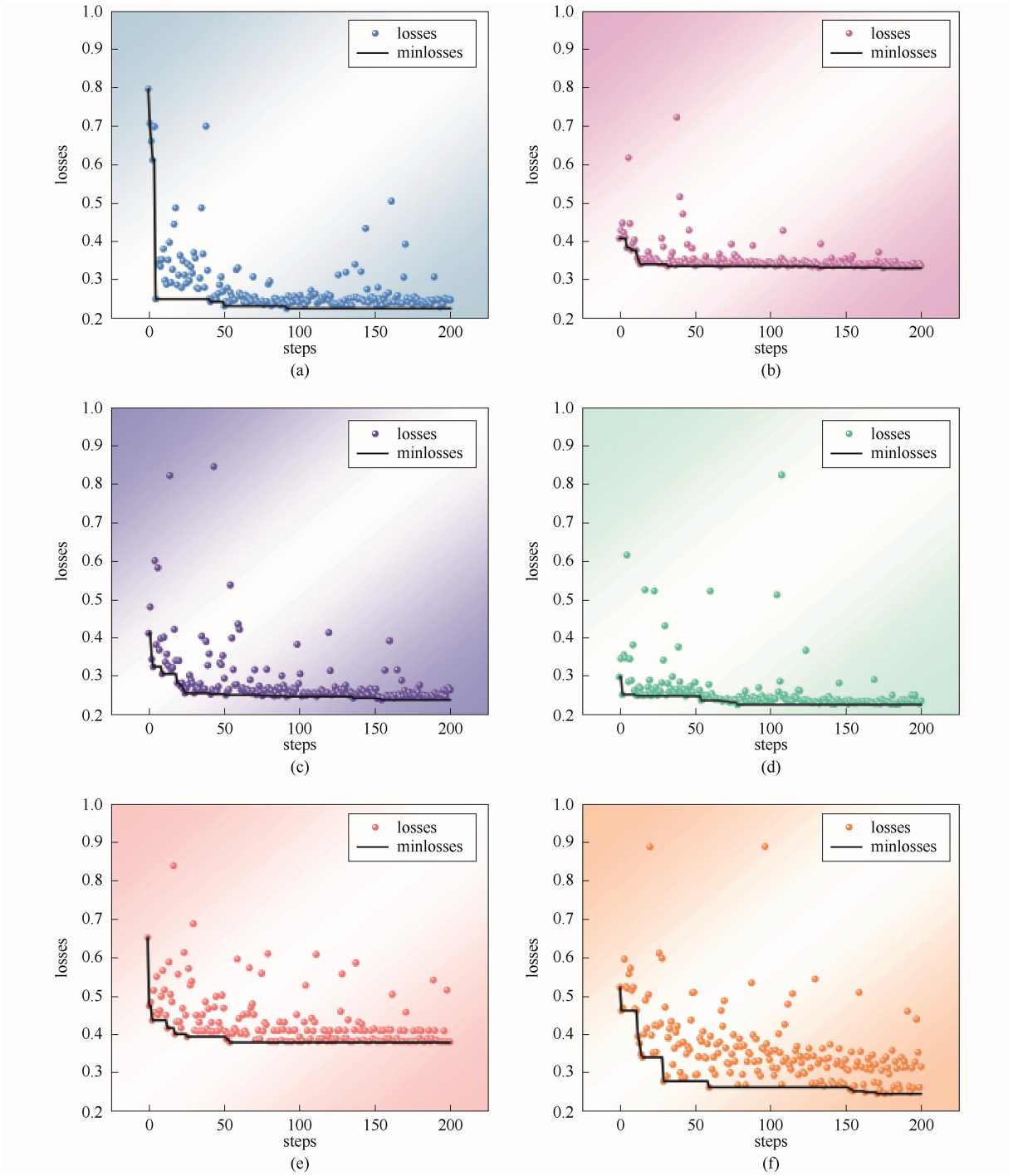


Fig. 4. Hyperparameter optimization history curves of various ensemble learning models: (a) CatBoost; (b) AdaBoost; (c) LGBM; (d) GBDT; (e) RF; and (f) XGB.

3.2.3. Identification of the optimal ensemble learning model

The R^2 and RMSE are applied to quantitatively compare the predictive performance of various ensemble learning models of the ammonia decomposition process, as shown in Table 2. Moreover, the fitting plot of the true values and the predicted values of X_{NH_3} and STY_{H_2} is also drawn to visually assess the predictive performance of each model, as shown in Fig. 6 and Fig. S3.

For the prediction of X_{NH_3}, the CatBoost model demonstrates the best performance, with a testing set R^2 value as high as 0.9203 and an RMSE of 6.8618. The scatter plot shows that the data points are highly concentrated and closely clustered around the $y = x$ perfect fit line, with the red fitting line almost coinciding with it, visually demonstrating the model's outstanding ability to capture complex nonlinear relationships. This is attributed to its advantages in handling mixed data types and its unique ordered boosting mechanism. Secondly, the GBDT model has a relatively high testing set R^2 of 0.9089. In contrast, the AdaBoost model has the poorest prediction performance, with a test set R^2 of only 0.8699, and its RMSE is relatively high (5.53). The scatter plot shows that the data points are relatively scattered, especially at the

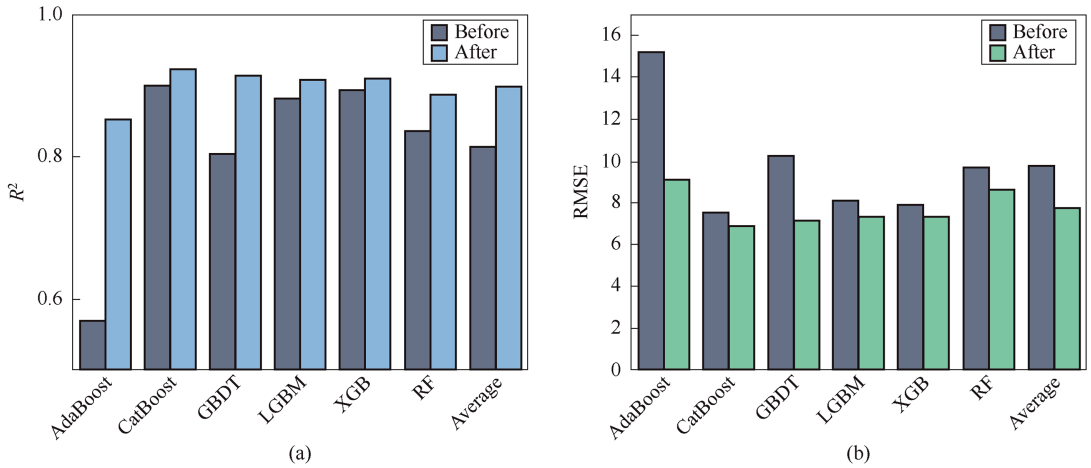


Fig. 5. Comparison of performance indicators of various ensemble learning models before and after hyperparameter tuning: (a) R^2 and (b) RMSE.

Table 2
Comprehensive comparison of the prediction performance of six ensemble learning models.

Output	Indicator	CatBoost	GBDT	LGBM	AdaBoost	XGBoost	RF
X_{NH_3}	R^2_{train}	0.9968	0.9962	0.9845	0.9788	0.9948	0.9766
	R^2_{test}	0.9203	0.9089	0.9061	0.8618	0.9059	0.8820
	$RMSE_{train}$	1.9030	2.0767	4.2050	4.9150	2.4354	5.1313
	RMS_{Etest}	9.6387	10.3052	10.4592	12.6924	10.4708	11.9171
STY_{H_2}	R^2_{train}	0.9975	0.9956	0.9862	0.9820	0.9947	0.9777
	R^2_{test}	0.9188	0.9192	0.9089	0.8451	0.9140	0.8947
	$RMSE_{train}$	0.7723	1.0234	1.8135	2.0728	1.1227	2.2360
	RMS_{Etest}	4.0032	3.9942	4.2397	5.5300	4.1210	5.3601

two ends of the predicted values, which are significantly deviated from the $y = x$ line. The red fitting line also has a large deviation.

For the prediction of STY_{H_2}, the CatBoost model also demonstrates outstanding comprehensive performance. Although its test set R^2 (0.9188) is very close to that of the GBDT model (R^2 = 0.9192), the CatBoost model stands out with the lowest RMSE value (4.4763), indicating its stronger robustness in providing more accurate predictions and reducing prediction errors. The scatter plot clearly shows that the predicted points of CatBoost are highly concentrated and closely clustered around the $y = x$ line, demonstrating an excellent fitting effect. In contrast, the AdaBoost model still performs the weakest in the prediction of STY_{H_2}, with a test set R^2 of only 0.8523. The scatter plot reveals obvious dispersion, with the predicted points significantly deviating from the ideal fitting line, especially in the low-value region where the degree of dispersion is more pronounced. This once again highlights the limitations of AdaBoost on the current dataset, resulting in significant prediction bias and insufficient reliability.

In summary, the multi-dimensional evaluation results show that compared with the other five prediction models, the constructed CatBoost model demonstrates the best accuracy in predicting the two key outputs (X_{NH_3} and STY_{H_2}) of the ammonia decomposition process. This is mainly because CatBoost demonstrates its unique advantages in handling categorical features. Compared with other models, CatBoost can natively and robustly handle categorical features through its unique Ordered Target Encoding and symmetric tree structure, effectively avoiding the risks of prediction drift and information leakage. Although LightGBM also supports native handling of categorical features, CatBoost's ordered boosting mechanism provides a more robust learning method. However, this enhanced robustness sometimes comes with higher training time, especially when dealing with large-scale datasets. Considering the scale of the dataset and the superior predictive performance, this study ultimately selects CatBoost as the main model for subsequent analysis and optimization.

3.3. Feature importance analysis based on SHAP

3.3.1. Feature importance analysis of ammonia conversion

Fig. 7(a) clearly presents the ranking of feature importance of each input feature for the ammonia conversion (X_{NH_3}). Among them, the influence of reaction conditions is the most significant, accounting for as high as 56.14%; followed by the intrinsic properties of the catalyst, which accounts for 30.12%; while the impact of catalyst preparation parameters is relatively small, only accounting for 13.73%. These proportions are the average main effect contribution rate of the entire reaction condition, catalyst intrinsic property, and preparation parameter groups calculated based on SHAP values rather than interaction mechanism importance. In this regard, it should be noted that the significance of catalyst preparation parameters (such as the preparation method) is often reflected indirectly through their interaction with intrinsic properties (such as catalyst size and specific surface area). Although the contribution rate of the main effect of this parameter group is relatively low, it still has a decisive influence on activity by regulating the microstructure of the catalyst.

From the perspective of specific features, the reaction temperature plays a crucial role in the ammonia decomposition process, aligning with its endothermic nature. According to Le Chatelier's Principle, increasing the temperature shifts the equilibrium towards the product side, thereby improving ammonia

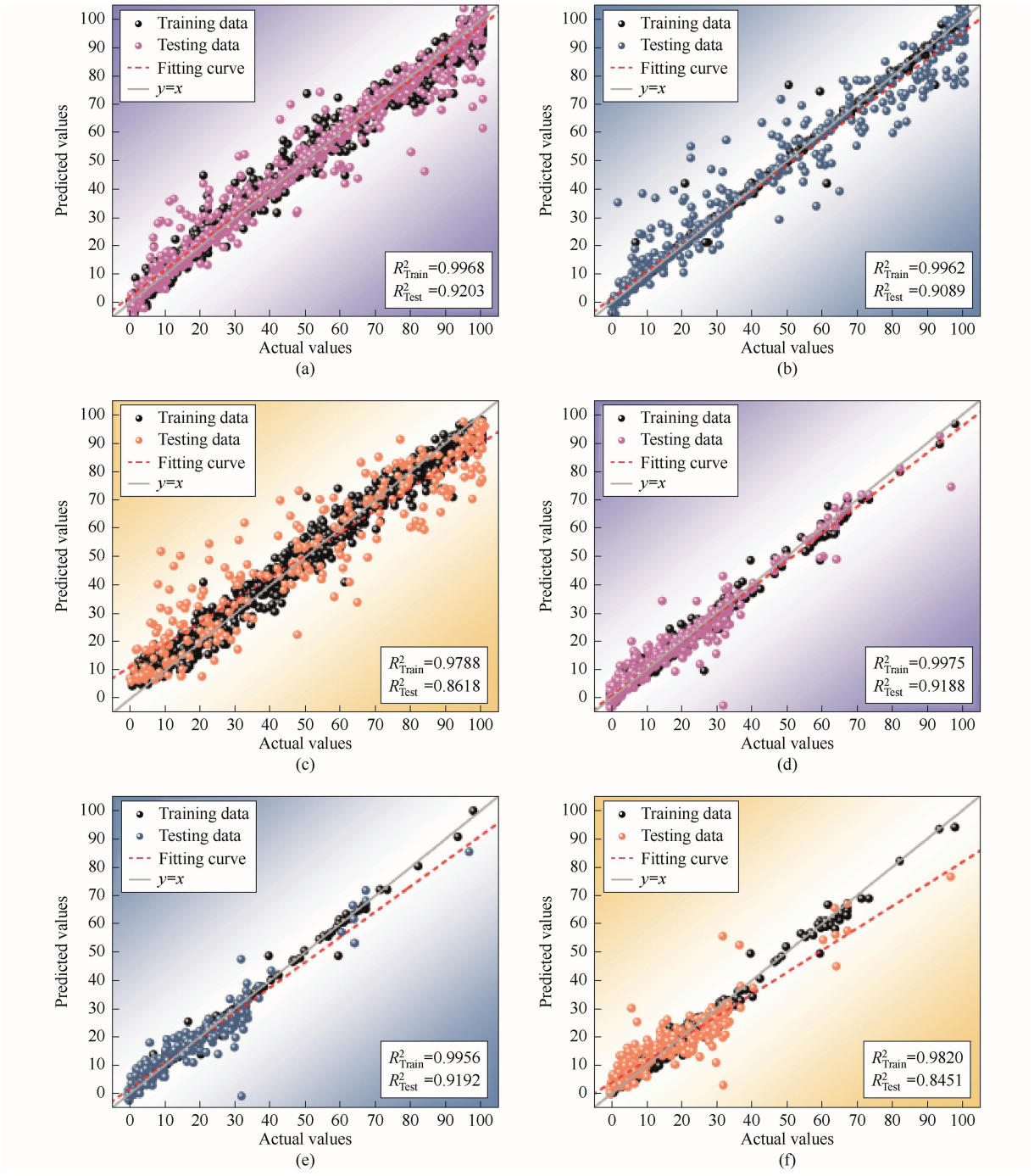


Fig. 6. Comparison of the fitting results of the CatBoost ((a), (d)), GBDT ((b), (e)), and AdaBoost ((c), (f)) models on the training and testing sets: (a)–(c) ammonia conversion ratio and (d)–(f) STY_{H_2} (Those of the rest model are indicated in Fig. S3).

conversion. Higher temperatures positively influence reaction kinetics, speeding up the reaction and allowing it to reach equilibrium more quickly. This is consistent with the relationship between temperature and reaction rate described by the Arrhenius equation, which shows that a rise in temperature accelerates the reaction and boosts conversion efficiency, as depicted in Fig. 7(b). Moreover, high temperature can also effectively promote the adsorption and activation of ammonia molecules on the catalyst surface, and overcome the high activation energy required for the cleavage of N—H bonds and the desorption of N_2, thereby driving the entire catalytic cycle forward [6]. GHSV is the second most important input feature for ammonia decomposition due to it directly determines the residence time of reactants on the active sites of the catalyst. A lower GHSV means a longer contact time, allowing ammonia molecules more sufficient time to decompose on the catalyst surface, thereby increasing the conversion rate. A longer residence time ensures that reactant molecules have sufficient opportunities to fully contact the active sites of the catalyst

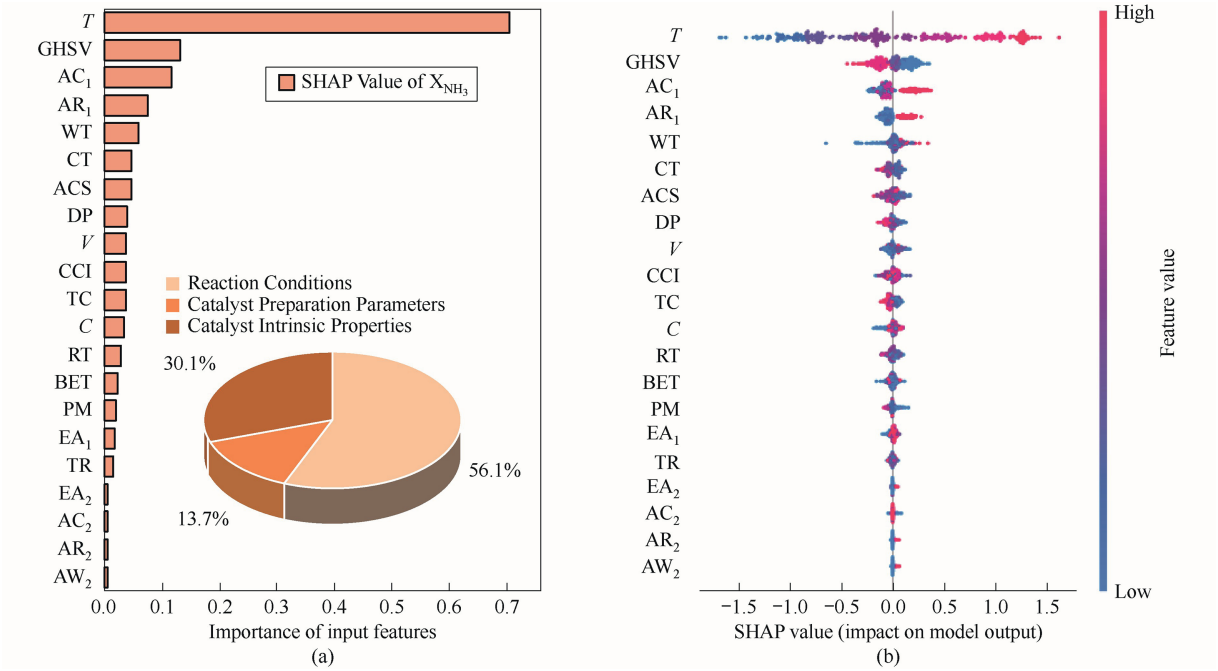


Fig. 7. Analysis of the influence of input features on X_{NH_3} based on SHAP: (a) ranking of the average SHAP value-based importance of input features and (b) SHAP-based bee swarm plot.

and undergo effective reactions, thereby enhancing the utilization rate of the active sites and the conversion efficiency of ammonia molecules [10]. This is further confirmed on the 10(b) SHAP swarm plot, where GHSV shows a significant negative correlation with X_{NH_3}. Furthermore, the active component and its atomic radius in the intrinsic properties of the catalyst, as well as the total metal loading, are also of great significance for ammonia decomposition. This is mainly because the type of active component determines the adsorption strength and electronic interaction between the catalyst and reactants and products. For instance, metals with moderate N adsorption strength usually exhibit higher catalytic activity because they can facilitate the effective cleavage of N—H bonds without overly binding N atoms [10]. Atomic radius indirectly affects the geometric structure of active sites and steric hindrance effects. The total metal loading is directly related to the number of available active sites on the catalyst surface and the dispersion of metals. Therefore, increasing the metal loading can provide more catalytic active centers within a certain range by accelerating the activation and decomposition of ammonia molecules. However, an excessively high loading may lead to sintering of metal particles or coverage of active sites, which in turn reduces the catalytic efficiency. Therefore, considering the contributions and correlations of various features, more efforts should be devoted to appropriately increasing the reaction temperature and the total metal loading, as well as reducing the GHSV, in order to enhance the ammonia conversion ratio.

3.3.2. *Feature importance analysis of space-time yield of hydrogen*

The feature importance and correlation of each input feature on the hydrogen generation rate (STY_{H_2}) are indicated in Fig. S4(a) and (b). From the perspective of overall contribution, reaction conditions still play a dominant role, accounting for 42.30%; the intrinsic properties of the catalyst rank second, with a contribution of 32.99%; the contribution of catalyst preparation parameters is 24.72%. Thus, although the reaction conditions remain important, their significance has decreased from 56.14% to 42.30% compared to X_{NH_3}. The main reason is that the physical and chemical processes characterized by X_{NH_3} and STY_{H_2} are different. The formation of X_{NH_3} is mainly controlled by thermodynamic equilibrium and intrinsic reaction kinetics. The reaction temperature directly affects the reaction rate constant through the Arrhenius equation, and an increase in temperature is conducive to overcoming the high activation energy barrier of N—H bond cleavage, promoting the reaction to move towards the product side. GHSV determines the completion degree of surface reactions by regulating the residence time of reactants at active sites. Therefore, the contribution of reaction conditions to X_{NH_3} is relatively high. STY_{H_2} is not only determined by the conversion ratio but also strongly depends on the feedstock flux per unit time and the number of effective active sites of the catalyst. Although increasing the temperature can enhance the intrinsic rate, an excessively high GHSV will shorten the contact time and limit the single-pass conversion rate, thereby partially offsetting the positive effect of temperature on STY_{H_2}. Furthermore, STY_{H_2} is more susceptible to the modulation of catalyst structural parameters such as specific surface area and pore volume, which affect the diffusion of reactants and the accessibility of active sites. Therefore, the contribution of reaction conditions relatively decreased (42.30%), while the intrinsic properties (32.99%) and preparation parameters (24.72%) significantly increased, demonstrating that STY_{H_2} is more sensitive to the coupling effect of catalyst structure and operating conditions than X_{NH_3}.

Specifically, the reaction temperature remains the most significant factor influencing STY_{H_2}, ranking first in its impact. The SHAP swarm plot further reveals the specific positive correlation between reaction temperature and STY_{H_2}, as shown in Fig. S4(b). Therefore, appropriately increasing the reaction temperature will be conducive to enhancing the STY_{H_2}. Calcination time follows closely, as a key parameter in catalyst preparation, directly affecting the formation of crystal phases, grain size, pore structure, and the stability and dispersion of active components, thereby determining the intrinsic activity and hydrogen generation rate of the catalyst. Moreover, it shows a negative correlation trend, which means that appropriately lowering the calcination

temperature will be conducive to improving STY_{H_2}. It is because that appropriately lowering the calcination temperature helps maintain the high dispersion of active components, suppresses grain growth and sintering, and forms a pore structure that is more conducive to the adsorption of reactants and the desorption of products, thereby optimizing the specific surface area and the exposure of active sites of the catalyst. Reduction temperature ranks third, having a significant impact on the formation of active metal phases, metal dispersion, grain size, and the generation of surface defects in the catalyst. However, the negative correlation of reduction temperature indicates that a higher reduction temperature will lead to material sintering, a reduction in active sites and structural damage, thereby lowering the catalytic performance and suppressing the hydrogen generation rate. It is due to that excessively high reduction temperatures will accelerate the migration and coalescence of metal nanoparticles, leading to severe sintering and ultimately inhibiting the activation of ammonia and the generation of hydrogen. In addition, the total metal loading is also an important factor affecting STY_{H_2}, as more active metals mean more active sites participating in the reaction, thereby increasing the space-time yield of hydrogen per unit time. Therefore, appropriately raising the reaction temperature and the total metal loading, while reducing the calcination and reduction temperatures, could significantly increase the STY_{H_2} of the ammonia decomposition reaction.

3.4. Analysis of the interaction relation between key features and targets of ammonia decomposition reaction

To identify the synergistic or antagonistic effects among input features and outputs, PDP analysis is further utilized to visually analyze the interaction relationship between the most important input features determined by SHAP and these outputs.

3.4.1. Effect of key features on ammonia conversion

The effect of the GHSV, the atomic radius of the first active component, and the total metal loading on the ammonia conversion ratio (X_{NH_3}) are shown in Fig. 8(a) and (b). As GHSV increases, X_{NH_3} generally shows a downward trend, especially when GHSV exceeds approximately 25200 $ml \cdot h^{-1} \cdot (g\ cat)^{-1}$, X_{NH_3} shows a more significant decreasing trend, as shown in Fig. 8(a) and (b). This is mainly due to the significant reduction in the residence time of reactants at the active sites of the catalyst, which leads to insufficient decomposition of ammonia molecules. However, although a lower GHSV (for example, less than approximately 12600 $ml \cdot h^{-1} \cdot (g\ cat)^{-1}$) theoretically can achieve a higher conversion rate, the processing capacity of the catalyst per unit volume and time is small, and the production capacity of the equipment cannot be fully utilized, indirectly increasing the equipment investment cost. The atomic radius of the first active component shows an overall positive correlation with X_{NH_3}. The influence of the total metal content on the ammonia conversion ratio is characterized by a significant increase from 5% to 15% and then stabilizing. Because increasing the metal loading in this ranges can effectively enhance the density of active sites on the catalyst surface, promoting the activation and decomposition of ammonia molecules. However, when the loading exceeds 15%, the active sites may become saturated, and even due to the sintering of metal particles or the steric hindrance effect between active sites, the active area may no longer increase significantly. Therefore, a GHSV range of 12600 to 25200 $ml \cdot h^{-1} \cdot (g\ cat)^{-1}$ and a WT range of 5% to 15% are recommended to achieve a balance between maintaining a high conversion rate and achieving a high space-time yield, while also maximizing the conversion ratio.

3.4.2. Effect of key features on space-time yield of hydrogen

The effect of total metal loading (WT), reduction temperature (RT), and calcination time (TC) on the space-time yield of hydrogen (STY_{H_2}) is indicated in Fig. 9(a) and (b). The STY_{H_2} generally shows an upward trend with the increase of WT as shown in Fig. 10(a). Although STY_{H_2} continues to rise after WT exceeds 10%, its growth rate is significantly lower than the rapid increase of WT within the range of 0% to 5%. The RT shows a negative correlation with STY_{H_2}, especially within the temperature range of 400 °C to 500 °C, where STY_{H_2} drops rapidly. This might be due to the fact that when RT exceeds a certain temperature (approximately 400 °C) and continues to rise, the excessively high temperature accelerates the sintering and agglomeration of active metal nanoparticles, resulting in a significant reduction in the specific surface area of the catalyst and a decrease in the density of effective active sites. Fig. 9(b) shows that within the calcination time of 0 to 3 h, a relatively high STY_{H_2} is maintained; however, further extending the TC leads to a gradual decline in STY_{H_2}. This is mainly due to the fact that as the TC is prolonged further (especially beyond 6 h), it exerts a destructive impact on the physical structure (specific surface area, pore channels, particle size) and chemical composition/valence state/interaction of the catalyst, thereby causing a significant decrease in STY_{H_2}. Long-term calcination may cause phase transformation or crystallization of the catalyst support, thereby reducing its specific surface area and porosity; meanwhile, the active metal components may undergo excessive oxidation, grain growth, or even form undesirable solid solutions with the support. These changes will reduce the effective active sites and alter their electronic properties, ultimately impairing the performance of the catalyst. In summary, response surface analysis quantitatively reveals the key nonlinear effects of critical preparation parameters such as total metal loading, reduction temperature, and calcination time on the STY_{H_2}. However, these key parameters should not be too large. For instance, when WT is within 0% to 10%, RT is between 400 °C and 600 °C, and TC is within 0–3 h, it can achieve a high reducibility and structural stability of the active metal phase as well as a high STY_{H_2}.

3.5. Multi-objective optimization ammonia decomposition catalyst

This study conducts multi-objective optimization aimed at identifying efficient new catalysts for ammonia decomposition, with the goal of achieving an optimal balance between economic viability (represented by total metal loading, WT) and hydrogen production efficiency (STY_{H_2}). Although ruthenium-based catalysts have long been regarded as the most active metal catalysts for ammonia decomposition, nickel-based and iron-based catalysts are currently the most commonly used in large-scale industrial applications. Therefore, this study focuses on the optimization and comparative evaluation of these three catalyst systems.

As shown in Fig. 10(a)–(c), this study systematically presents the solution space distribution characteristics and the Pareto optimal front of these three catalyst systems in the multi-objective optimization problem. This front clearly represents the inherent trade-off boundary between total metal loading and space-time yield of hydrogen, *i.e.*, at a given performance level, further simultaneous optimization of both parameters is not possible. It also fully characterizes the distribution pattern of the non-dominated solution set within the feasible solution space. Based on the theory of bi-objective optimization, the TOPSIS multi-criteria decision-making method is employed to perform trade-off analysis on each Pareto front to determine the optimal solution.

As for the iron-based catalyst, the feasible solution set exhibits a dense distribution within a broad parameter space of $STY_{H_2} \in [30, 90]$ $mmol \cdot (g\ cat)^{-1} \cdot min^{-1}$ and $WT \in [0\%, 90\%]$, as

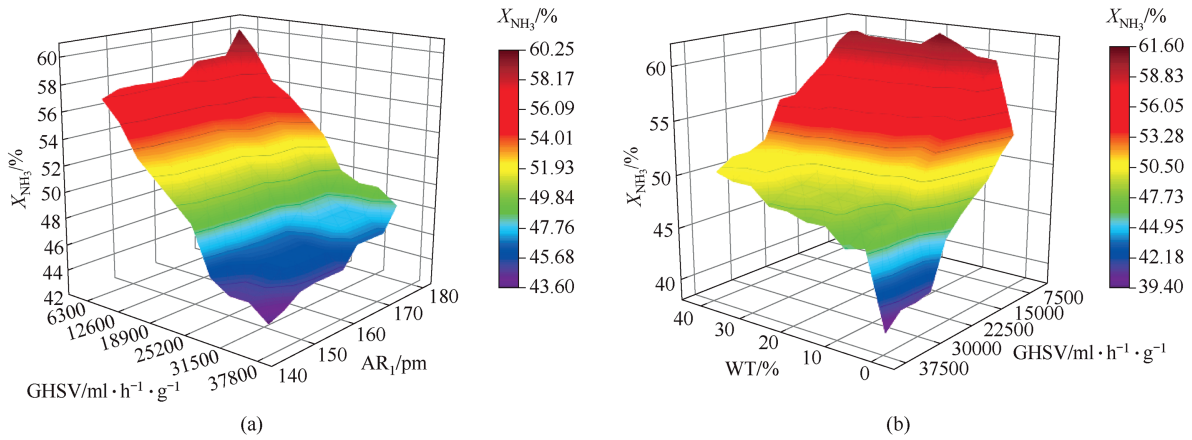


Fig. 8. PDPs of key input features on X_{NH_3}: (a) GHSV and AR_1, as well as (b) GHSV and WT.

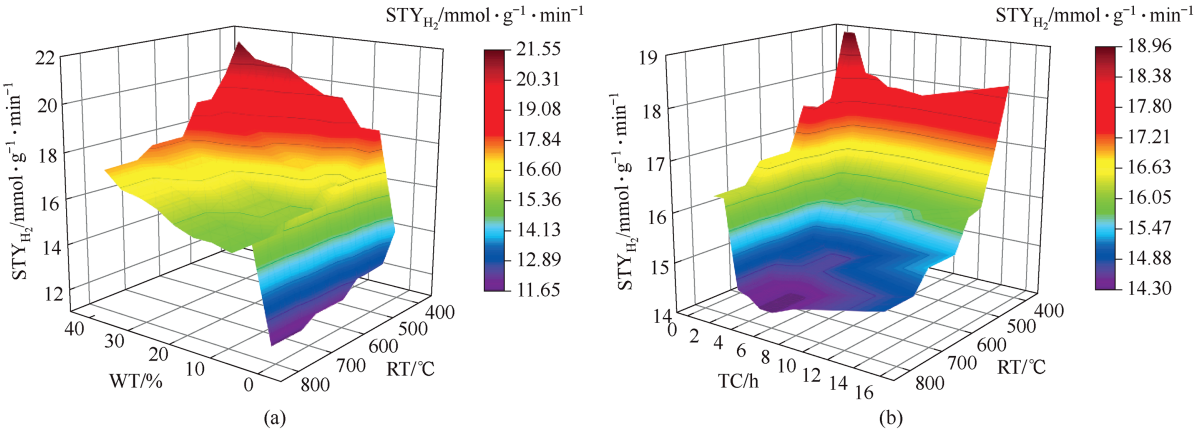


Fig. 9. PDPs of key input features on STY_{H_2}: (a) WT and RT as well as (b) TC and RT.

shown in Fig. 10(a). This indicates that the iron-based catalyst system has considerable design flexibility and optimization potential. The Pareto optimal frontier reveals that to achieve higher STY_{H_2} performance, a higher total metal loading is usually required. Therefore, to achieve a balance between economy and efficiency by ensuring a high STY_{H_2} while minimizing the WT of the catalyst as much as possible, the TOPSIS method is used to conduct a trade-off analysis on the Pareto frontier. The optimal solution coordinates ultimately identify the predicted Fe-K/MCF-17 catalyst, with a STY_{H_2} value of 76.02 mmol·(g cat)$^{-1}$·min^{-1} and a WT of 3.86%, as the most promising catalyst among the iron-based catalysts. The detailed information of this predicted catalyst is shown in Table S3. Fig. 10(b) illustrates the feasible solution set of nickel-based catalysts is relatively concentrated, mainly within the range of STY_{H_2} approximately 40 to 75 mmol·(g cat)$^{-1}$·min^{-1} and WT from 0% to 14%. Compared with iron-based catalysts, the overall STY_{H_2} and WT levels of nickel-based catalysts are slightly lower, and the distribution is more compact. This may reflect the relatively narrow optimization window for metal loading and active site regulation of nickel-based catalysts or their inherent catalytic performance limitations. As a result, the TOPSIS approach recommends that the predicted Ni/$LaAl_{12}O_{19}$ catalyst has the highest catalytic performance among the Ni-based catalyst, with a STY_{H_2} of 69.61 mmol·(g cat)$^{-1}$·min^{-1} and a WT of 6.57%. Similarly, this study identifies that the Ru-La/NiO is the most promising catalyst among ruthenium-based catalysts, with a STY_{H_2} of 65.51 mmol·(g cat)$^{-1}$·min^{-1} and a WT of 0.84%, as shown in Fig. 10(c). The detailed information of these three optimized catalysts is indicated in Table S3, which provide a clear basis for the experiment to verify the excellent catalysts obtained through computational design in this study.

To present the performance of the three predicted catalysts more intuitively, their performance is compared with the catalysts in the dataset, as shown in Fig. 10(d). The detailed information of these reported catalysts is shown in Table S4. As this study aims at a new type of ammonia decomposition catalyst with a lower total metal loading (WT) and a higher STY_{H_2}, the better the comprehensive performance of the catalyst, the closer it will be to the lower right corner of Fig. 10(d). Therefore, the results clearly show that the comprehensive performance of these three preferred catalysts is significantly superior to that of the remaining catalysts in the database. This strongly demonstrates the reliability and effectiveness of the multi-objective optimization process adopted in this paper in discovering high-performance ammonia decomposition catalysts. However, more experimental characterizations and tests will be needed, which will be the focus of our next research.

3.6. External validation with unseen experimental data

The optimized CatBoost model is systematically evaluated and validated using an independent experimental data to thoroughly

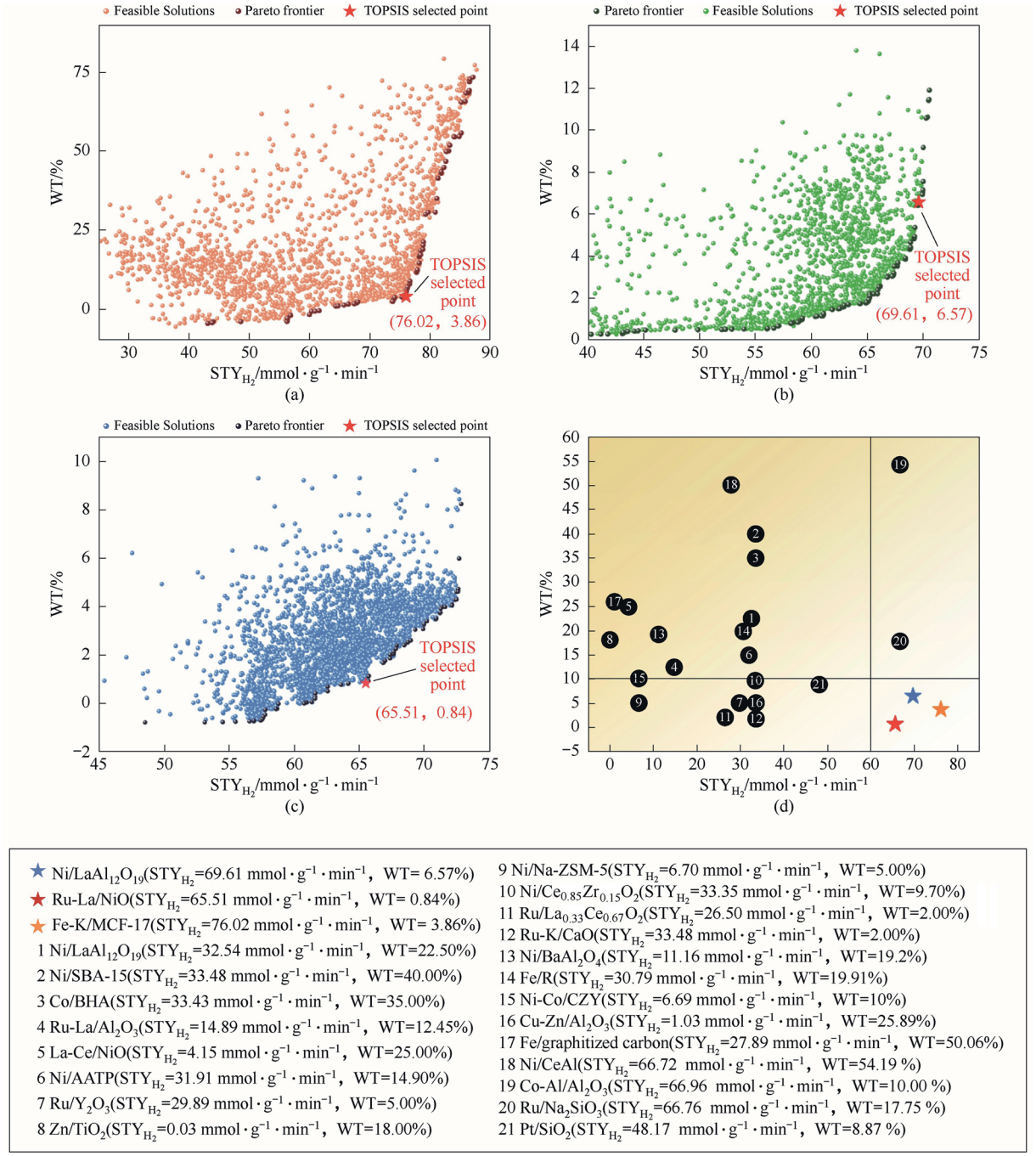


Fig. 10. Multi-objective optimization and performance evaluation of different metal-based catalysts: (a) Fe-based catalysts, (b) Ni-based catalysts, (c) Ru-based catalysts, and (d) performance comparison between the optimized catalysts and the reported catalysts.

assess its predictive accuracy, stability, and generalization capability, as illustrated in Fig. S5(a)–(c). Specifically, experimental data corresponding to the CoCe-NC catalyst reported by Kang *et al.* [36], the Ru/SiO_2(SC950) catalyst from Lee & Park [37], and Ni/CeO_2 catalyst reported by Zhang *et al.* [38] are employed as the validation set. It is important to note that these data are not involved in any stage of model training, thereby ensuring the objectivity and reliability of the validation outcomes. The results demonstrate that the optimized CatBoost model exhibits exceptional predictive performance, with predictions closely aligning with experimental trends. Notably, the maximum relative error between the predicted and measured values across all data points is only 5.06%, with the majority of errors remaining below 3%. These findings indicate that the established CatBoost model possesses high accuracy and stability, along with excellent generalization ability.

Despite the promising predictive performance demonstrated by the optimized CatBoost model, its performance relies heavily on feature representation and selection. Inadequate descriptor sets may fail to capture critical catalytic mechanisms, thereby limiting interpretability and physical relevance. To address these

challenges, future work should prioritize expanding the experimental database to incorporate a broader variety of input features, catalyst families, and reaction parameters. Additionally, it is important to incorporate time-dependent parameters and stability data into the CatBoost model to address transient behavior and enhance the practical applicability of its predictions. Ultimately, sustained collaboration between computational modeling and experimental validation will be essential to achieve robust and universally applicable catalyst design frameworks.

4. Conclusions

This study develops a Bayesian optimization-driven interpretable ensemble learning framework that advances ammonia decomposition catalyst design. This framework integrates six ensemble learning algorithms for effectively avoiding the limitations of a single model. Through an automated hyperparameter optimization strategy based on Optuna, all models exhibit asymptotic convergence, and their corresponding loss function values are significantly reduced. Especially, the CatBoost model, which demonstrates outstanding prediction accuracy ($R^2 = 0.9198$), is adopted as the core prediction engine for the design of ammonia decomposition catalysts. Its prediction mechanism is investigated by employing the SHAP and PDP analysis. The results demonstrate that reaction conditions play a dominant role in ammonia conversion, accounting for 56.14% of the total impact. In contrast, for hydrogen space-time yield, although reaction temperature remains the most influential factor, the importance of intrinsic catalyst properties (32.99%) and preparation parameters (24.72%) increases significantly. Finally, the optimal CatBoost model coupled with the RVEA algorithm is applied for intelligent search of new and efficient catalysts that achieve a better balance between catalyst cost and hydrogen space-time yield. Ultimately, three high-performance ammonia decomposition catalysts with various metal bases are successfully selected. In addition, external validation confirms <5.06% prediction error across unseen catalytic systems. Therefore, the proposed framework establishes a transferable paradigm for low-temperature, energy-efficient ammonia decomposition that bridges computational design and sustainable hydrogen production.

CRediT Authorship Contribution Statement

Zhao Wang: Writing – original draft, Visualization, Methodology, Investigation, Data curation. Jingsong Guan: Visualization, Resources, Investigation, Data curation. Jun Hu: Visualization, Validation, Data curation. Qiwen Guo: Writing – original draft, Validation. Dawei Zhang: Writing – review & editing, Project administration, Formal analysis. Qingchun Yang: Writing – review & editing, Supervision, Methodology, Conceptualization.

Declaration of Competing Interest

The authors declare that they have no known competing financial interests or personal relationships that could have appeared to influence the work reported in this paper.

Acknowledgements

The authors are grateful for financial support from the Natural Science Foundation of Anhui Province (2508085MB029), National Natural Science Foundation of China (22108052), and High-end chemicals and cutting-edge new materials Technology Innovation Center of Hefei (HCHC202309).

Supplementary Material

Supplementary data to this article can be found online at https://doi.org/10.1016/j.cjche.2026.01.006.

References

[1] S.C. Sun, Q.Q. Jiang, D.Y. Zhao, T.T. Cao, H. Sha, C.K. Zhang, H.T. Song, Z.J. Da, Ammonia as hydrogen carrier: advances in ammonia decomposition catalysts for promising hydrogen production, *Renew. Sustain. Energy Rev.* 169 (2022) 112918.
[2] J.E. Lee, J. Lee, H. Jeong, Y.K. Park, B.S. Kim, Catalytic ammonia decomposition to produce hydrogen: a mini-review, *Chem. Eng. J.* 475 (2023) 146108.
[3] T. Han, L. Wei, S.H. Xie, Y.X. Liu, H.X. Dai, J.G. Deng, Catalyst design for ammonia decomposition: an overview, *Ind. Chem. Mater.* 3 (3) (2025) 311–331.
[4] Y. Zhao, B.P. Setzler, J.H. Wang, J. Nash, T. Wang, B.J. Xu, Y.S. Yan, An efficient direct ammonia fuel cell for affordable carbon-neutral transportation, *Joule* 3 (10) (2019) 2472–2484.
[5] M. Perron, K. Krawczyk, M. Młotek, Plasma-catalytic decomposition of highly concentrated ammonia for a chemical hydrogen storage, *Chem. Eng. Sci.* 314 (2025) 121815.
[6] H.H. Fang, S. Wu, T. Ayvali, J.W. Zheng, J. Fellowes, P.L. Ho, K.C. Leung, A. Large, G. Held, R. Kato, K. Suenaga, Y.I.A. Reyes, H.V. Thang, H.T. Chen, S.C.E. Tsang, Dispersed surface Ru ensembles on MgO(111) for catalytic ammonia decomposition, *Nat. Commun.* 14 (2023) 647.
[7] X.C. Wang, X.T. Zhao, G.Z. Zhou, T. Chen, Q. Chen, N. Alonso-Vante, Z. Huang, Y.R. Zhang, H. Lin, Electrically driven gaseous ammonia decomposition for hydrogen production over SiC-mediated catalyst without external heating, *ACS Catal.* 15 (3) (2025) 2389–2401.
[8] M.Y. Yang, U. Raucci, M. Parrinello, Reactant-induced dynamics of lithium imide surfaces during the ammonia decomposition process, *Nat. Catal.* 6 (9) (2023) 829–836.
[9] C.Z. Zheng, B. Guan, J.F. Guo, T.X. Su, J.F. Zhou, J.Y. Chen, Y.Y. Zhang, Y.H. Yuan, W.K. Xie, N.X. Zhou, Z. Huang, Research status, optimization strategies, and future prospects of ammonia decomposition catalysts for CO_x-free hydrogen, *Ind. Eng. Chem. Res.* 62 (29) (2023) 11305–11336.
[10] H.W. Liu, R.R. Zhang, S.B. Liu, G.Z. Liu, CeO_2/Ni inverse catalyst as a highly active and stable Ru-free catalyst for ammonia decomposition, *ACS Catal.* 14 (13) (2024) 9927–9939.
[11] K. Xu, Y.Y. Zhang, W.W. Wang, M. Peng, J.C. Liu, C. Ma, Y.W. Zhang, C.J. Jia, D. Ma, C.H. Yan, Single-atom barium promoter enormously enhanced non-noble metal catalyst for ammonia decomposition, *Angew. Chem. Int. Ed.* 64 (4) (2025) e202416195.
[12] R.J. Bao, Z. Wang, Q.W. Guo, X.Y. Wu, Q.C. Yang, Bio-digital catalyst design: generative deep learning for multi-objective optimization and chemical insights in CO_2 methanation, *ACS Catal.* 15 (15) (2025) 12691–12714.
[13] Q.C. Yang, D.W. Rong, Q.W. Guo, R.J. Bao, D.W. Zhang, Ensemble learning-driven multi-objective optimization of the co-pyrolysis process of biomass and coal for high economic and environmental performance, *Chin. J. Chem. Eng.* 84 (2025) 23–34.
[14] Q.C. Yang, L. Zhao, Q.W. Guo, Z. Wang, D.W. Zhang, A hybrid encoding-enhanced machine learning and multioptimization framework for the optimal catalyst design of the methane-to-ethylene process, *Ind. Eng. Chem. Res.* 64 (29) (2025) 14512–14533.
[15] H.T. Cao, Y. Li, C.L. Chang, X.P. Zhang, A. Yang, W.F. Shen, A deep learning hybrid framework combining an efficient evolutionary algorithm for complex many-objective optimization of sustainable triple CO_2 feed methanol production, *ACS Sustainable Chem. Eng.* 12 (17) (2024) 6682–6696.
[16] C. Bozal-Ginesta, S. Pablo-García, C. Choi, A. Tarancón, A. Aspuru-Guzik, Developing machine learning for heterogeneous catalysis with experimental and computational data, *Nat. Rev. Chem* 9 (9) (2025) 601–616.
[17] A.F. Zahrt, J.J. Henle, B.T. Rose, Y. Wang, W.T. Darrow, S.E. Denmark, Prediction of higher-selectivity catalysts by computer-driven workflow and machine learning, *Science* 363 (6424) (2019) eaau5631.
[18] A. Yang, S.R. Sun, Y. Su, Z.Y. Kong, J.Z. Ren, W.F. Shen, Insight to the prediction of CO_2 solubility in ionic liquids based on the interpretable machine learning model, *Chem. Eng. Sci.* 297 (2024) 120266.
[19] W.J. Guo, A. Shafizadeh, H. Shahbeik, S. Rafiee, S. Motamedi, S.A. Ghafarian Nia, M.H. Nadian, F.H. Li, J.T. Pan, M. Tabatabaei, M. Aghbashlo, Machine learning for predicting catalytic ammonia decomposition: an approach for catalyst design and performance prediction, *J. Energy Storage* 89 (2024) 111688.
[20] X.M. Chen, A. Shafizadeh, H. Shahbeik, M.H. Nadian, M. Golvirdizadeh, W.X. Peng, S.S. Lam, M. Tabatabaei, M. Aghbashlo, Enhanced bio-oil production from biomass catalytic pyrolysis using machine learning, *Renew. Sustain. Energy Rev.* 209 (2025) 115099.
[21] S. Azadvar, O. Tavakoli, Data-driven interpretation, comparison and optimization of hydrogen production from supercritical water gasification of biomass and polymer waste: applying ensemble and differential evolution in machine learning algorithms, *Int. J. Hydrogen Energy* 85 (2024) 511–525.
[22] J. Kumar, G. Selvan, R. Saranya, R.K. Gupta, M. Anusuya, G. Kalra, Optimising silver-enhanced $BiFeO_3$ nanoparticle catalysts using random forests and genetic algorithms, in: 2024 International Conference on Distributed Systems,

Computer Networks and Cybersecurity (ICDSCNC). Bengaluru, India, IEEE, 2025, pp. 1–6.
[23] R.Y. Zuo, Y. Li, S.A. Wei, Z.M. Li, T. Shi, W.L. Du, W.F. Shen, Calibration-augmented and mechanism-driven deep learning hybrid framework for modeling actual distillation processes, *Ind. Eng. Chem. Res.* 64 (7) (2025) 3856–3870.
[24] J. Zhang, Q. Wang, Y. Su, S.M. Jin, J.Z. Ren, M. Eden, W.F. Shen, An accurate and interpretable deep learning model for environmental properties prediction using hybrid molecular representations, *AIChE J.* 68 (6) (2022) e17634.
[25] N.S. Lai, Y.S. Tew, X.L. Zhong, J. Yin, J.L. Li, B.H. Yan, X.N. Wang, Artificial intelligence (AI) workflow for catalyst design and optimization, *Ind. Eng. Chem. Res.* 62 (43) (2023) 17835–17848.
[26] D.W. Rong, Z. Wang, Q.W. Guo, R.J. Bao, Q.C. Yang, An auto-configurable and interpretable ensemble learning framework for optimal catalyst design of green methanol production *via* Bayesian optimization, *J. Clean. Prod.* 488 (2025) 144666.
[27] S.H. Nan, Z.M. Li, S.M. Jin, W.L. Du, W.F. Shen, Machine learning-based multimodal and multi-granularity feature fusion framework for accurate prediction of molecular properties, *Ind. Eng. Chem. Res.* 64 (5) (2025) 3045–3056.
[28] Q.C. Yang, R.J. Bao, D.W. Rong, J.X. Xiao, J.L. Zhou, L. Zhao, D.W. Zhang, Interpretable machine learning for accelerating reverse design and optimizing CO_2 methanation catalysts with high activity at low temperatures, *Ind. Eng. Chem. Res.* 63 (33) (2024) 14727–14747.
[29] Z.H. Jaffari, A. Abbas, S.M. Lam, S. Park, K. Chon, E.S. Kim, K.H. Cho, Machine learning approaches to predict the photocatalytic performance of bismuth ferrite-based materials in the removal of malachite green, *J. Hazard. Mater.* 442 (2023) 130031.
[30] S.Y. Jiang, W. Xu, Q. Xia, M. Yi, Y.R. Zhou, J.W. Shang, X.W. Cheng, Application of machine learning in the study of cobalt-based oxide catalysts for antibiotic degradation: an innovative reverse synthesis strategy, *J. Hazard. Mater.* 471 (2024) 134309.
[31] C. Martínez-Alonso, V. Vassilev-Galindo, B.M. Comer, F. Abild-Pedersen, K.T. Winther, J. Llorca, Application of machine learning to discover new intermetallic catalysts for the hydrogen evolution and the oxygen reduction reactions, *Catal. Sci. Technol.* 14 (13) (2024) 3784–3799.
[32] M.F. Tahir, M.Z. Yousaf, A. Tzes, M.S. El Moursi, T.H.M. El-Fouly, Enhanced solar photovoltaic power prediction using diverse machine learning algorithms with hyperparameter optimization, *Renew. Sustain. Energy Rev.* 200 (2024) 114581.
[33] L. Salt, M. Gallagher, Hyperparameter optimisation with practical interpretability and explanation methods in probabilistic curriculum learning, arXiv: 2504.06683 (2025), https://doi.org/10.48550/arXiv.2504.06683.
[34] T. Terlouw, C. Bauer, R. McKenna, M. Mazzotti, Large-scale hydrogen production *via* water electrolysis: a techno-economic and environmental assessment, *Energy Environ. Sci.* 15 (9) (2022) 3583–3602.
[35] Y.X. Wu, A.C.Y. Yuen, C.M. Mo, Q. Chen, X.Y. Huang, An advanced BPNN/RVEA coupled control strategy for novel immersed liquid cooling battery thermal management system, *J. Energy Storage* 125 (2025) 117008.
[36] B. Kang, Z.L. Chang, R.D. Zhang, Z.G. Shen, K. Wang, X.N. Guo, H.T. Wu, D.Q. Li, D.X. Liu, Y. Wei, J.B. Jia, Z.J. Wang, Synergistic catalysis of CoN sites and Co nanoparticles for efficient CO x-free hydrogen production from ammonia decomposition, *Fuel* 396 (2025) 135311.
[37] H.J. Lee, E.D. Park, Ammonia decomposition over Ru/SiO_2 catalysts, *Catalysts* 12 (10) (2022) 1203.
[38] Z. Zhang, M.H. Yu, M.Q. Shen, W. Li, G.R. Shen, Promoting effect of alkaline earth metals on Ni/CeO_2 catalysts for ammonia decomposition reaction, *Mol. Catal.* 578 (2025) 115016.